Journal of Drug Delivery Science and Technology 107 (2025) 106813

Contents lists available at ScienceDirect

Journal of Drug Delivery Science and Technology

journal homepage: www.elsevier.com/locate/jddst

Subcutaneous administration of an endocrine-mimetic, slow-release protein material reduces the severity of SARS-CoV-2 infection

Eloi Parladé [a,b,c,1], Ferran Tarrés-Freixas [d,e,f,1], Marianna T.P. Favaro [b,c], Jara Lascorz [b,c], Merce Márquez-Matínez [b,c], Rosa Mendoza [b,c], José Luís Corchero [a,b,c], Guillermo Cantero [d,e], Núria Roca [d,e], Mónica Pérez [d,e], Neus Ferrer-Miralles [a,b,c], Esther Vazquez [a,b,c], Joaquim Segalés [d,g], Júlia Vergara-Alert [d,e,*], Antonio Villaverde [a,b,c,**]

[a] Departament de Genètica i de Microbiologia, Universitat Autònoma de Barcelona, Plaça Cívica s/n, Bellaterra, Barcelona, 08193, Spain
[b] Institut de Biotecnologia i de Biomedicina, Universitat Autònoma de Barcelona, Plaça Cívica s/n, Bellaterra, Barcelona, 08193, Spain
[c] CIBER de Bioingeniería, Biomateriales y Nanomedicina (CIBER-BBN), Barcelona, 08193, Spain
[d] Unitat Mixta d'Investigació IRTA-UAB en Sanitat Animal, Centre de Recerca en Sanitat Animal (CReSA), Campus de la Universitat Autònoma de Barcelona (UAB), Bellaterra, Spain
[e] IRTA, Programa de Sanitat Animal, CReSA, Campus de la Universitat Autònoma de Barcelona (UAB), Bellaterra, Spain
[f] University of Vic-Central University of Catalonia (UVic-UCC), Catalonia, 08500, Vic, Spain
[g] Department de Sanitat i Anatomia Animals, Facultat de Veterinària, Campus de la UAB, Bellaterra, Spain

ARTICLE INFO

Keywords:
Recombinant protein
Biomaterial
Slow-release vaccine
SARS-CoV-2
Amyloid

ABSTRACT

Slow-antigen release vaccination systems aim to replicate the prolonged antigen exposure occurring during natural viral infections, which usually last for days or weeks. We have developed a Zn-assisted, self-organizing protein material at the microscale, inspired by the granular depots for protein hormones, that slowly disassembles into functional building block polypeptides under physiological conditions. This endocrine-like platform acts as a dynamic protein depot for prolonged protein release. Having been validated in oncology, regenerative medicine, and in antimicrobial peptide delivery, it also shows promise for immune stimulation. Here, we evaluate, for the first time, whether such artificial secretory granules incorporating the SARS-CoV-2 Spike Receptor Binding Domain (RBD) can elicit a protective immune response against viral challenge in golden Syrian hamsters. The antigen, formulated as secretory granules, was administered in varying doses via intranasal or subcutaneous routes. While the formulations did not prevent infection, they enhanced viral clearance and mitigated body weight loss, particularly with subcutaneous administration. These effects, through the subcutaneous route, were achieved even in the absence of an adjuvant. Additionally, the granules triggered both antigen-specific humoral immunity and antigen-independent immunomodulatory effects, potentially linked to their amyloid-like structure. These findings demonstrate the dual mechanism of this platform, activating both adaptive and innate immune pathways, and its potential as a versatile, adjuvant-free system for enhancing immune responses against infectious diseases.

1. Introduction

Biocompatible delivery systems enabling the sustained release of functional molecules from a single administration are of great interest in chemical therapies to minimize the peak-and-valley drug level oscillations [1–3]. Such approaches enhance drug efficacy, space doses over time, and minimize potential toxicities associated with over-threshold drug levels. Different types of materials have been developed to act as

* Corresponding author. Unitat Mixta d'Investigació IRTA-UAB en Sanitat Animal, Centre de Recerca en Sanitat Animal (CReSA), Campus de la Universitat Autònoma de Barcelona (UAB), Bellaterra, Spain.
** Corresponding author. Institut de Biotecnologia i de Biomedicina, Universitat Autònoma de Barcelona, Plaça Cívica s/n, Bellaterra, Barcelona, 08193, Spain.
E-mail addresses: julia.vergara@irta.cat (J. Vergara-Alert), antonio.villaverde@uab.cat (A. Villaverde).
[1] Equally contributed.

https://doi.org/10.1016/j.jddst.2025.106813
Received 29 August 2024; Received in revised form 18 February 2025; Accepted 12 March 2025
Available online 13 March 2025

drug-hosting scaffolds, allowing slow and/or regulatable drug release [4–7]. However, like drug carrier nanoparticles, the holding material can pose toxicity concerns, both in the patient and in the environment [8]. Therefore, clinically applicable drug-hosting materials should be non-toxic and biodegradable. In fact, ideally, the drug itself should be packaged in self-contained, self-disassembling structures that release their building blocks over time, without the need of any chemically heterogeneous carrier molecules, cages or matrices [8].

Nature provides inspiration for such structures in the form of functional amyloids [9–11]. On the one hand, the mechanical stability of amyloids derives from the coordination between cationic zinc (Zn^{2+}) and histidine residues [12–14]. On the other hand, the cross connectivity between protein chains occurs through Zn-stabilized amyloidal patches, whose formation is fully reversible under physiological conditions [15,16]. Among functional amyloids, bacterial inclusion bodies [10], and granular depots of protein hormones [17,18] are microscale protein clusters that have guided the construction of synthetic equivalents [19,20]. In particular, the granular structure and release mechanics of insulin and growth hormones is being progressively solved [12,18,21], and it offers clues for the *in vitro* generation of industry-oriented, mimetic protein materials [22]. Artificially constructed amyloids, like their natural counterparts [16,23], release the building block protein in a time-sustained way, both *in vitro* [24] and upon subcutaneous administration [25], through a progressive disassembly process mainly regulated by a physiological process of Zn chelation [26] that lasts for a few weeks [25]. These synthetic secretory granules are spontaneously formed *in vitro* when, upon purification or chemical synthesis, a hexahistidine (H6) tagged polypeptide is mixed with Zn salts that provide the divalent form of the metal [26]. The crosslinking mediated by the divalent cationic Zn creates stable but reversible bonds between chains [27], that can be disrupted by soluble histidine or by chelators such as EDTA [28]. Progressively increasing amounts of Zn^{2+} promote the formation of simple oligomeric structures at the nanoscale and more complex granules at the microscale [29]. Although the microparticles are mechanically stable [19], under physiological conditions they slowly disintegrate, probably by Zn dilution. During the disintegration process, protein oligomers in the nanoscale have been often observed [29], suggestive of a step-based disassembling process.

The clinical potential of synthetic functional amyloidal depots as sustained delivery systems has been demonstrated in oncology by subcutaneous administration [19,30], in regenerative medicine on *in vitro* wound models [31] and in stem cell culture [32], and in microbiology through oral delivery of antimicrobial peptides [33]. Recent studies aimed at the evaluation of the potential toxicity of synthetic protein granules upon subcutaneous administration [34] have revealed significant humoral [34–36] and cellular immune responses [36] elicited against the protein forming the granules. However, whether the protein release kinetics from administered granules might induce an efficient protective response against a viral challenge has not been studied. While the temporal profile in which an antigen is exposed has been observed as critical for immune activation [37], the fine regulation of protein release from synthetic secretory granules need to be approached. To explore if the complex immunological responses observed upon granule administration [36] could be functional to protect against infections by viral pathogens, we developed a SARS-CoV-2 vaccine prototype and tested it in animal models. Current RNA-based anti-SARS-CoV-2 vaccines have been instrumental in controlling the COVID-19 pandemic [38], but protein-based approaches are still under consideration facing the high post-pandemic SARS-CoV-2 infection incidence [39,40] and the fast evolution of the virus [41]. Our data indicate that while the tested prototypes do not prevent infection, they serve as powerful immunogens that reduce convalescence time, even when administered as single doses without adjuvants. Beyond their utility as sustained antigen delivery systems, our data also suggest antigen-independent immunomodulatory effects, warranting further examination and offering promise for the application of this new protein-based material in a wide spectrum of immuno-prophylactic approaches.

2. Materials and methods

2.1. Protein production and microgranule preparation

The gene encoding an extended version of the receptor binding domain (eRBD) of the SARS-CoV-2 spike protein was designed in-house and synthesized by GeneArt (Thermo Fisher, Waltham, MA, USA). Antigen production, purification, and characterization were performed as detailed elsewhere [42]. Briefly, eRBD was produced in *Escherichia coli* BL21 DE3 cells upon induction by isopropyl-β-d-1-thiogalactopyranoside (IPTG) and subsequent solubilization and refolding of the resulting inclusion bodies. The recombinant protein GFP-H6, intended for use in the mock formulation, was produced in *Escherichia coli* Origami B cells (BL21, *ompT, lon, TrxB*, Gor–; Novagen) and purified by Ni^{2+}-based affinity chromatography as previously described [29]. After obtaining both recombinant proteins, microparticles were generated through a controlled process involving the interaction of the soluble protein with ionic Zn [34]. Shortly, the soluble his-tagged antigen was mixed with zinc chloride in a potassium-sodium phosphate-buffered saline (PBS) solution at pH 7.4. The reaction was allowed to proceed for 10 min to ensure proper protein-cation interaction and aggregation. Following this step, the mixture was centrifuged at 15,000×*g* for 15 min to remove the non-aggregated soluble protein from the formed microgranules.

2.2. Virus isolates

Viral challenge in hamsters was performed with a B.1 (D614G) SARS-CoV-2 (*Betacoronavirus pandemicum*) isolate obtained from an oropharyngeal swab of a COVID-19 patient in Spain (April 2020). The production of viral stocks, as well as the isolation and titration processes, were performed using Vero E6 cell (ATCC® CRL-1586™). Virus titration was performed on 96-well plates using the Reed-Muench method, and results were expressed as TCID50/mL [43].

2.3. Animal handling and vaccination

All animal procedures were performed under the approval of the ethical committees of *Institut de Recerca en Tecnologia Agroalimentaria* (IRTA) and *Institut de Recerca Germans Trias i Pujol* (IGTP), and with the authorization of Generalitat de Catalunya (CEA-OH/11894/1, internal CEEA IRTA code 330–2020). Eight week-old golden Syrian hamsters (GSH, n = 56; 0.5 male/female ratio) were purchased from Envigo (Indianapolis, IN, US), and they were housed in the specific pathogen free (SPF) facilities at *Centre de Medicina Comparativa i Bioimatge* (CMCiB-IGTP). Hamsters were distributed in groups of 2–3 animals/cage (same sex) and fed *ad libitum* in cycles of 12 h (h) light/dark and stable temperature and relative humidity.

Animals (n = 12/group) were vaccinated with 100 μl of three different vaccine regimens: i) one dose of microgranule-eRBD complex (100 μg of antigen in PBS) intranasally (IN); ii) one dose of microgranule-eRBD complex (300 μg of antigen in PBS) subcutaneously (SC1); iii) two doses (3-week interval) of microgranule-eRBD complex (100 μg of antigen) adjuvanted with 50 % (v/v) AddaVax (InvivoGen, San Diego, CA, USA) subcutaneously (SC2A). Control groups were: (a) unvaccinated, uninfected (n = 4); (b) unvaccinated, infected (n = 12); and (c) mock vaccinated (1 dose of 100 μg microgranule-GFP-H6 complex in PBS) subcutaneously (n = 4). All GSH were weighted on a weekly basis and monitored once a day until challenge. One week after the second vaccination, animals were moved to the animal Biosafety Level-3 (aBSL-3) facilities in IRTA-CReSA. Animals were housed in the same groups from origin (CMCiB-IGTP), and in the same environmental conditions, and one week after acclimatation they were challenged with

1000 TCID50/animal of the abovementioned SARS-CoV-2 isolate. Animals were followed-up for 7 days and they were euthanized on 2-, 4-, and 7-8-days post-inoculation (dpi). Humane endpoint criteria included a 20 % body weight loss, and/or the presence of severe clinical signs. Upon euthanasia, blood and oropharyngeal swabs were collected. Afterwards, animals were necropsied, and lungs and nasal turbinates (NT) were harvested for virological and histopathological analyses.

For virological analyses, a small fragment from the left apical lobule was collected in 0.5 mL DMEM +1 % penicillin/streptomycin. Subsequently, tissue was disaggregated with a TissueLyser II (QIAGEN), centrifuged at 1000 relative centrifugal units (rcf), and supernatant recovered. For histopathological analyses, tissues were fixed by immersion in a 10 % formalin solution for 7 days prior processing.

2.4. RNA-extraction and quantitative RT-qPCR

Viral RNA was extracted from the recovered supernatant of homogenized organs (nasal turbinate and lungs) and oropharyngeal swab samples using the IndiMag pathogen kit (Indical Bioscience) on a Biosprint 96 workstation (QIAGEN) according to the manufacturer's instructions and as previously reported [44]. Briefly, RT–qPCR targets a portion of the envelope protein gene (position 26,141–26,253 of GenBank NC_004718). The primers and probes used, and their final concentration are the follow: forward: 5′-ACAGGTACGTTAATAGTTAATAGCGT-3′ [400 nM], reverse: 5′-ATATTGCAGCAGTACGCACACA-3′ [400 nM] probe: 5′-FAM-A-CACTAGCCATCCTTA CTGCGCTTCG-TAMRA-3′ [200 nM]. Thermal cycling was performed at 55 °C for 10 min for reverse transcription, followed by 95 °C for 3 min and then 45 cycles of 94 °C for 15 s, 58 °C for 30 s.

2.5. Histology

Formalin-fixed upper (NT) and lower (lung) respiratory tract tissues from GSH were subjected to histopathological processing. Hematoxylin and eosin (H&E) staining was employed, and resultant slides were examined under an optical microscope. A semi-quantitative scoring system considering both the extent of inflammation and the severity of lesions was used to evaluate each sample. Scores ranged from 0 (no inflammation) to 3 (severe inflammation). The score assignment was conducted by a pathologist certified by the European College of Veterinary Pathologists (ECVP) and scoring was performed in a blinded fashion [44,45].

2.6. Enzyme-linked immunosorbent assay

The humoral response against SARS-CoV-2 was measured using an enzyme-linked immunosorbent assay (ELISA) performed on serum samples from blood collected on euthanized animals on 2, 4, and 7–8 dpi, as described elsewhere [35]. For the analysis we employed the Recombivirus Mouse Anti SARS-CoV-2 (COVID) Spike 1 RBD IgG ELISA Kit (RV-405420 Alpha Diagnostics, San Antonio, TX, USA), following the manufacturer's instructions.

2.7. Microscopy

High-resolution images of the eRBD microparticles were obtained using a Zeiss Merlin (Zeiss, Oberkochen, Germany) field-emission scanning electron microscope (FESEM). The microscope operated at 1 kV, and the excited electrons were collected using a high-resolution secondary electron detector. Sample preparation involved depositing 10 μL of microparticles suspension (0.1 mg/ml) onto a silicon wafer (Ted Pella Inc., Redding, CA, USA) and allowing it to dry at room temperature before direct observation. No metallic coating was applied.

2.8. Data analysis and structure prediction

Statistical analyses were performed using GraphPad Prism version 8.0.2 (GraphPad Software, San Diego, CA, USA). Differences between groups were analyzed using the Kruskal-Wallis's test, followed by Dunn's multiple comparisons test. Data are presented as mean and standard deviation or with individual data points, with statistical significance set at $p < 0.05$. The protein tridimensional structure was predicted from the amino acid sequence using Alphafold 3 [46].

3. Results and discussion

The RBD of the SARS-CoV-2 virus (Fig. 1A) was produced in different cell factories, including bacterial, insect, and mammalian cells, as described elsewhere [42]. While mammalian and insect cell-derived proteins were produced in insufficient amounts for *in vivo* testing, the H6-tagged eRDB (Fig. 1A) was successfully produced in bacteria, efficiently aggregating into protein-leaking microparticles in the presence of ionic Zn (Fig. 1B). The bacterial product was then formulated into granular particles for testing as a vaccine candidate against SARS-CoV-2 challenge. It should be noted that antigen-specific antibodies were elicited using eRBD-based secretory granules in mice [35], and a similar protein preparation based on the African swine fever virus (ASFV) antigen (p30) in pigs [36]. However, the effectiveness of these materials as vaccine components against viral infections has not been so far tested. For this purpose, we administered antigen-based granules (Fig. 1C) either subcutaneously (as previously tested) or intranasally (a yet untested administration route) and subsequently challenged the vaccinated animals (Fig. 1D). Given the sustained protein release features of the material, we included a single-shot protocol in our analyses and explored whether the microscale formulation could eliminate the need for an adjuvant, representing a step toward a more sustainable and cost-effective vaccination approach.

The administration of the vaccine prototypes did not affect body weight evolution (Fig. 2A) in agreement with the previously reported absence of toxicity of secretory granules [34]. Upon challenge with SARS-CoV-2, no clinical signs were observed besides an evident weight loss. The body weight evolution was similar in both vaccinated and unvaccinated groups (Fig. 2B), suggesting that the administered material did not prevent infection. However, significant differences in body weight were indeed observed during the recovery period from 4 dpi onwards (Fig. 2B). Notably, the recovery period was shorter in all vaccinated groups, including those exposed to the mock vaccine (GFP-H6), compared to the unvaccinated group. This result suggested a mild but evident antiviral effect associated with granule administration that appears to be antigen independent. The survival graph (Fig. 2C) illustrates that most subjects endured through both the vaccination and challenge phases, except for two animals, one from the unvaccinated and infected group, and one from the intranasally vaccinated (IN) cohorts, which were ethically euthanized in accordance with humane endpoint standards. These subjects were part of the same cohorts that exhibited a statistically significant weight loss compared to the control group.

To further explore the performance of the administered granules, a qPCR-based virological analysis was conducted on samples from the nasal turbinate, oropharynx (oropharyngeal swab), and lung. Initially, the viral load in all the samples was similar (Fig. 3A). However, a numerical analysis of viral load reduction revealed a faster decrease in the vaccinated groups compared to unvaccinated animals, with the clearance slopes being consistently higher in the immunized hamsters (Fig. 3B). This trend was consistent across all analyzed samples, except for those from the oropharynx, where this statement was only valid for the group administered subcutaneously with granules in the absence of adjuvant. The histological analysis of lesions in the target tissue did not reveal significant differences or splitting tendency between groups (Fig. 4). Specifically, SARS-CoV-2 inoculated hamsters developed

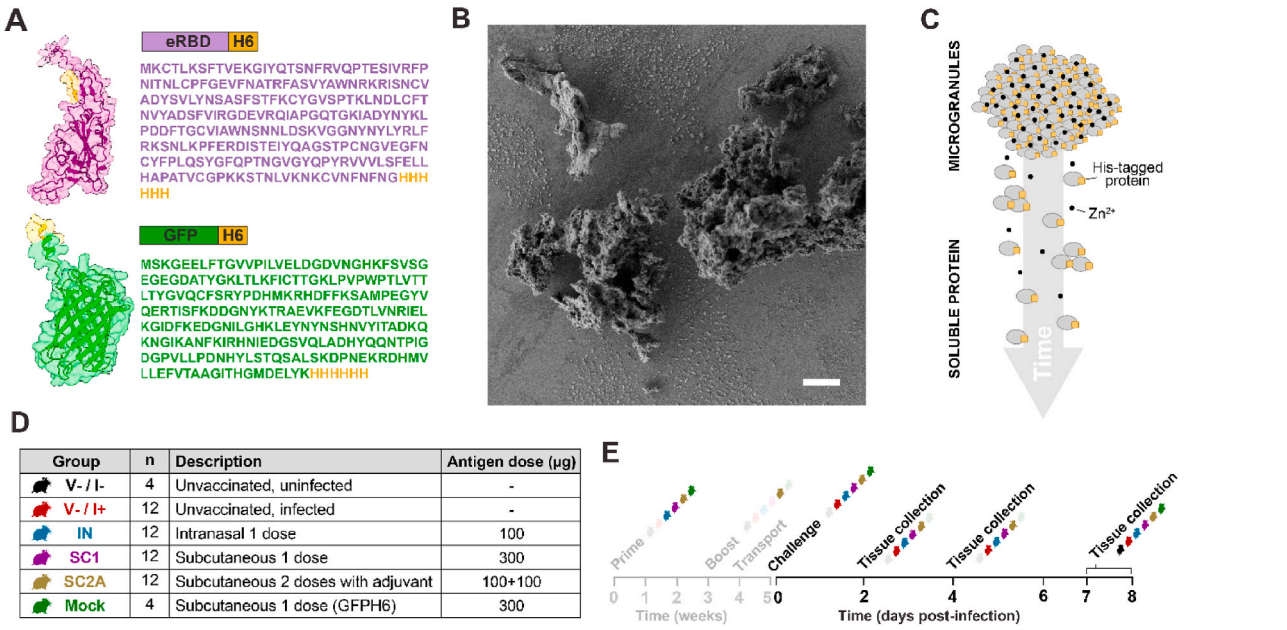

Group	n	Description	Antigen dose (µg)
V-/I-	4	Unvaccinated, uninfected	-
V-/I+	12	Unvaccinated, infected	-
IN	12	Intranasal 1 dose	100
SC1	12	Subcutaneous 1 dose	300
SC2A	12	Subcutaneous 2 doses with adjuvant	100+100
Mock	4	Subcutaneous 1 dose (GFPH6)	300

Fig. 1. Experimental design. A. Tridimensional structure prediction, domain organization and amino acid sequence of eRBD-H6 (top) and GFP-H6 (bottom), as described elsewhere [42]. B. Representative FESEM image of secretory granules. Scale bar represents 10 µm. C. Schematic representation of the protein leakage process from the microscale secretory granules. D. Organization of animal groups, administration routes and vaccine dosages. Mock vaccine was GFP-H6 [29] formulated as eRDB-H6. E. Assay timeline indicating vaccine administration regimens, challenge, and sample analyses.

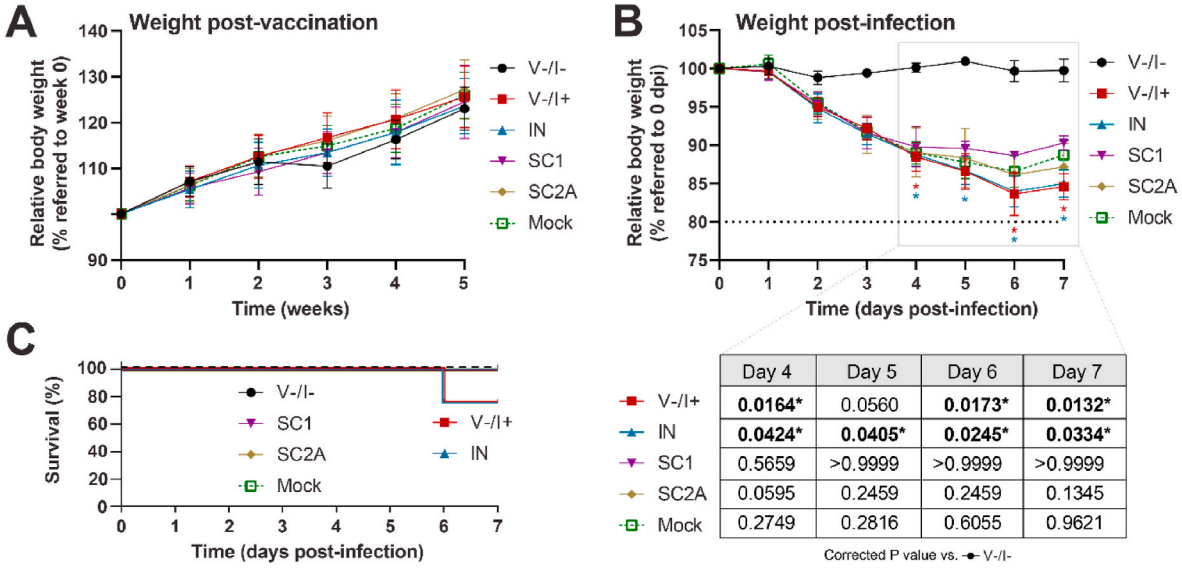

	Day 4	Day 5	Day 6	Day 7
V-/I+	**0.0164***	0.0560	**0.0173***	**0.0132***
IN	**0.0424***	**0.0405***	**0.0245***	**0.0334***
SC1	0.5659	>0.9999	>0.9999	>0.9999
SC2A	0.0595	0.2459	0.2459	0.1345
Mock	0.2749	0.2816	0.6055	0.9621

Corrected P value vs. V-/I-

Fig. 2. Body weight and survivability. A. Body weight evolution of GSH during the five weeks post-vaccination. B. Body weight evolution of GSH one-week post-challenge with SARS-CoV-2. The inset table shows the p-values from pairwise body weight mean comparisons between each experimental group and the uninfected group, with significant (*, $p < 0.05$) values highlighted in bold. C. Survival rates of GSH one-week post-challenge.

variable degrees of muco-purulent rhinitis and broncho-interstitial pneumonia, in a decreasing and increasing severity over time, respectively, as previously reported [44]. Examples of the histopathological scoring system are displayed in Fig. 5.

The observed results, particularly the body weight variation upon challenge (Fig. 2 B) and viral clearance (Fig. 3B), indicated that while the administration of the clustered protein did not protect against experimental infection, it positively influenced recovery. The fact that the mock vaccine (the irrelevant GFP antigen, Fig. 1A) also reduced convalescence time (Fig. 2B) and slightly enhanced viral clearance (as indicated by the steeper slope of viral clearance in 2 out of the 3 tissues tested, Fig. 3B) suggests some positive effects of granule administration that are antigen independent. In this regard, the antibody response against the viral protein was evaluated in all animal groups at 2 and 7–8 dpi (Fig. 6, top), indicating an antigen-dependent humoral response that was dose-dependent. Upon infection, the anti-RBD antibody levels tended to be homogeneous among all infected animal groups (Fig. 6, bottom).

The RBD is one of the most important targets for vaccination strategies. It can be incorporated into subunit vaccines, a safe and effective approach capable of inducing both humoral and cellular responses. This has been demonstrated in multiple pre-clinical trials using RBD-based formulations in different mammalian species, as well as in clinical trials [47,48]. Considering the economic feasibility challenges associated

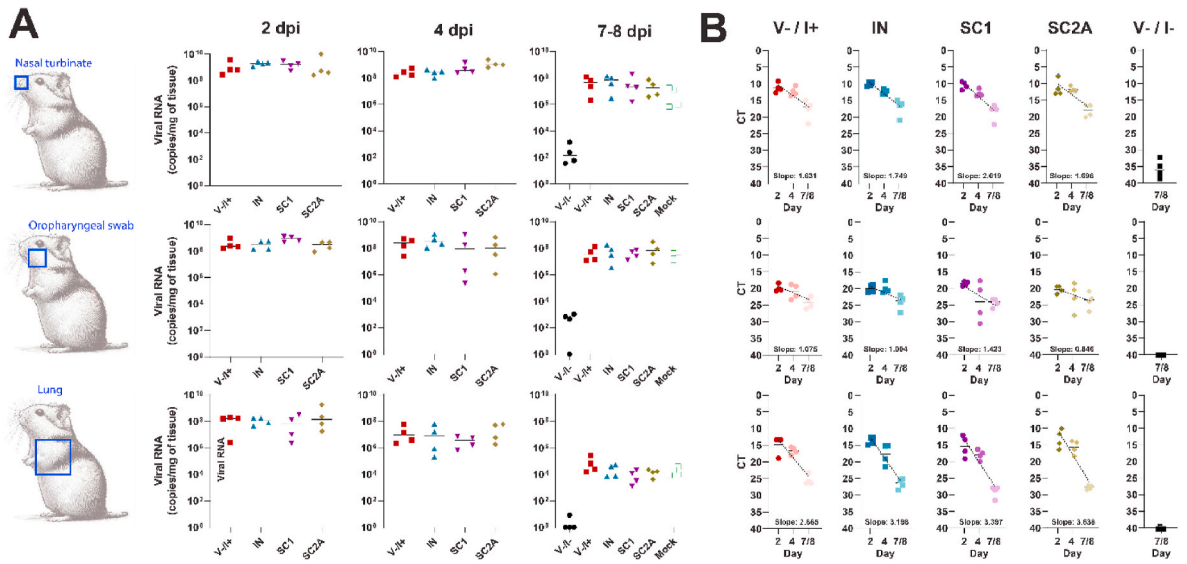

Fig. 3. Virological analyses. A. Titers of genomic RNA determined by qPCR from nasal turbinate (top), oropharynx (middle) and lung (bottom) tissue samples extracted at different times post-challenge. B. Comparative kinetics of viral clearance in unvaccinated and vaccinated groups.

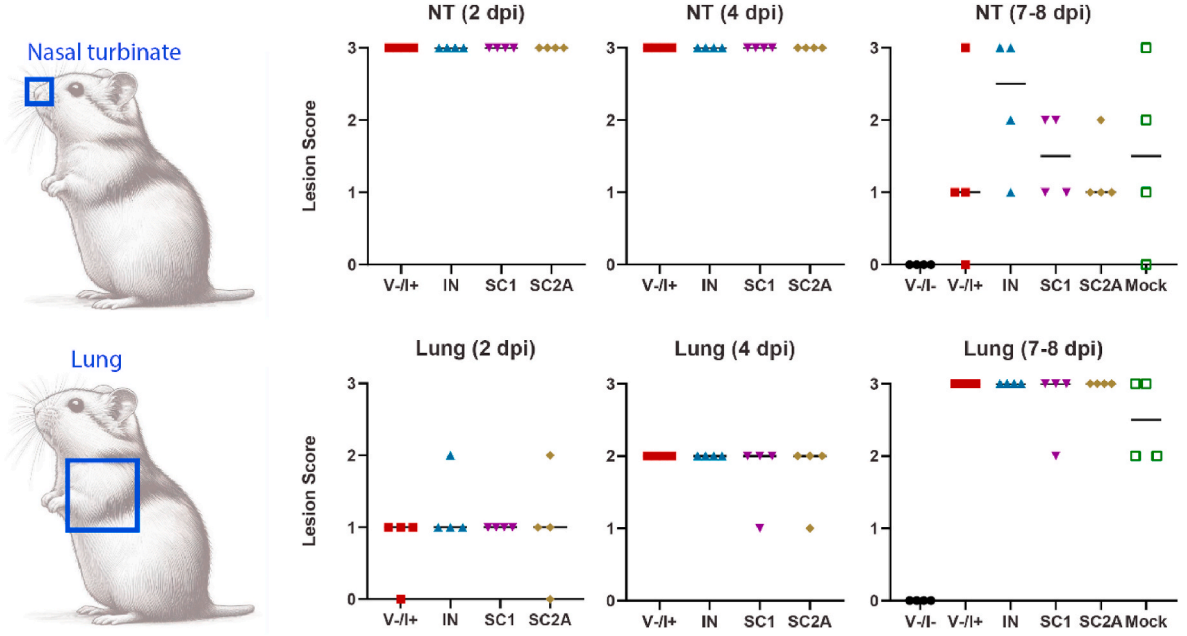

Fig. 4. Histological analysis of lesions in the nasal turbinate (top) and lung (bottom) tissues. Lesion scores indicate lack of lesions (0) or mild (1), moderate (2) or severe (3) inflammation.

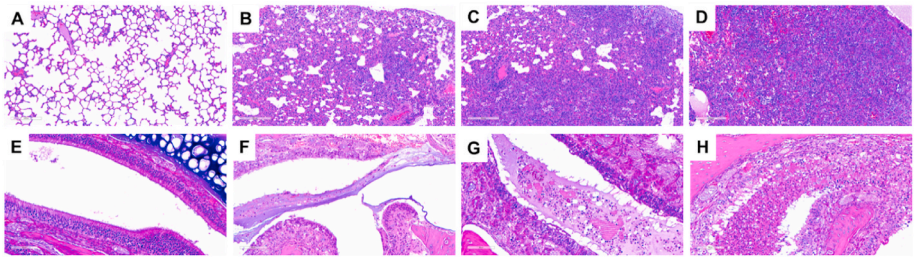

Fig. 5. Golden Syrian hamster lungs (A–D) and nasal turbinates (E–H) representing lesion scores 0 (no lesion, A and E), 1 (mild lesion, B and F), 2 (moderate lesion, C and G) and 3 (severe lesion, D and H). Damaged lungs display variable severity of a broncho-interstitial pneumonia, multifocal to diffuse, and affected nasal turbinates show an increasing severity of muco-purulent rhinitis. Hematoxylin & Eosin stain. (For interpretation of the references to colour in this figure legend, the reader is referred to the Web version of this article.)

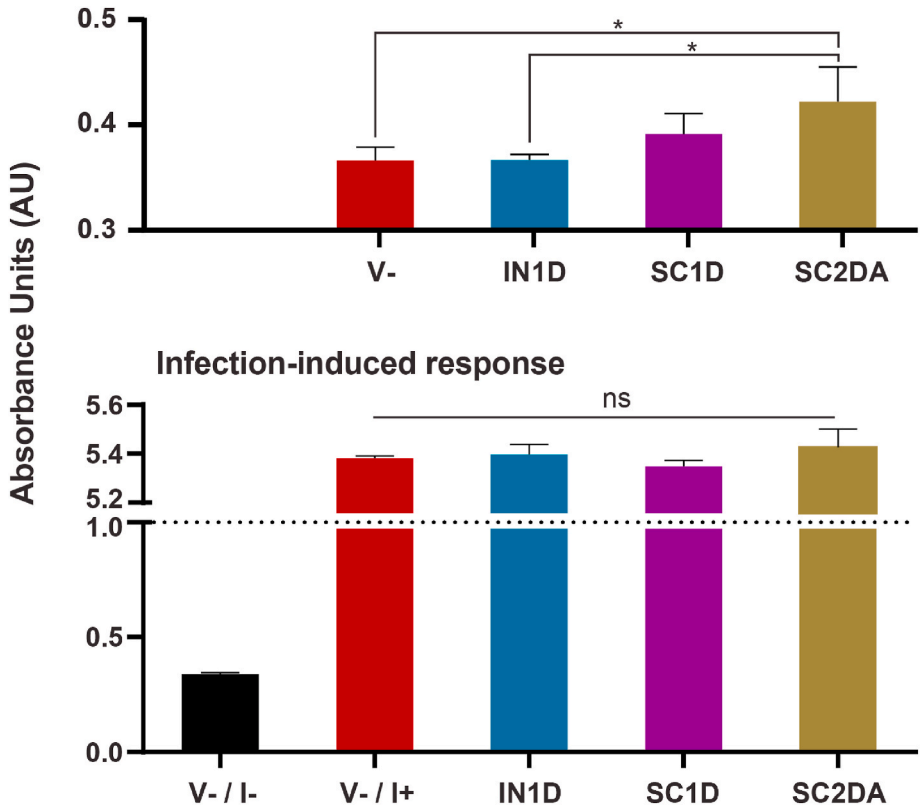

Fig. 6. Humoral immune response elicited by vaccination (top, 2 dpi) or infection by SARS-CoV-2 (bottom, 7–8 dpi) was evaluated using an anti-SARS-CoV-2 ELISA IgG kit with sera extracted at different time points. The dotted line represents the threshold for a positive humoral response. Statistical significance (*) was determined at $p < 0.05$.

with subunit vaccines, which can be limited by high production costs, we focused on using *E. coli*-produced antigens in this study. Specifically, we employed nano- and microparticles since these can enhance antigen presentation. Notably, previous reports have demonstrated that protein-only spike nanoparticles can boost neutralizing antibody responses and promote Th2 immunity in a Middle East respiratory syndrome coronavirus (MERS-CoV) vaccine [48,49]. The high cost of vaccines contributes significantly to global inequities in distribution and low coverage, particularly in low-income countries [50]. Therefore, prioritizing the development of cost-effective, prokaryotic-expressed subunit vaccines could help address these disparities and improve vaccine accessibility worldwide.

The data presented here points out artificial secretory granules, which mimic functional amyloids in the mammalian endocrine system, as potential vaccine candidates active upon viral challenge. As in other anti-SARS-CoV-2 vaccines that do not induce sterilizing immunity [51], the administration of the protein material did not prevent viral infection and replication but attenuated weight loss (Fig. 2B) and promoted faster viral clearance (Fig. 3B). The overall data is indicative of a dual effect of the formulation, namely triggering an antigen-dependent immune response (Fig. 6) and a protective effect that is irrespective of the antigenic formulation (Fig. 2B), as it was observed in hamsters that received an irrelevant GFP material version. Previous immunization data with a similar secretory material releasing a main antigen of ASFV [36] suggested the triggering of an innate cellular immune response associated with the protein format rather than its antigenic profile. It is well known that the unwanted aggregation of systemic protein drugs, intended to act in a soluble form, triggers undesired immune responses elicited by this aggregated state versus the non-immunogenic soluble version [52–54], potentially minimizing the therapeutic action. The biochemical or biological bases of such mechanisms are not well understood and are difficult to evaluate [55]. In this regard, the precise mechanism by which secretory granules interact with innate immune responses remains to be fully elucidated and is beyond the scope of this study. However, non-specific immune modulation has been described for other stimuli, such as β-glucan, LPS, and the bacillus Calmette–Guérin (BCG) vaccine, that can induce trained immunity responses [47,56]. This concept refers to the long-term functional reprogramming of innate immune cells, which leads to an altered response towards a second challenge after returning to a non-activated state [57].

In contrast to spontaneous protein aggregation that might occur during protein drug storage or administration, controlled Zn-assisted protein cross-linking by means of coordination with histidine residues generates internally structured functional amyloids [19,58] with semi-regular morphometric parameters [59], which offer both endocrine-like secretion properties and aggregation-linked immune stimulation. Importantly, this protein depot platform is self-contained and self-delivered, aligning with the “taking the vehicle out of drug delivery” principle [8], as it does not involve any external chemically heterogeneous container material. The results obtained in the present study indicate the proper functioning of secretory granules as dynamic depots and are highly supportive of slow and progressive antigenic availability, likely time sustained. Although it is not possible to monitor the release kinetics *in vivo*, the fact that one single dose of the packaged antigen shows a prolonged beneficial effect, at the organic level (Fig. 1B), indicates a slow protein release. Importantly, it occurs in absence of toxicity (Fig. 1A), showing that Zn doses used for protein packaging are, as expected, far below the threshold considered as save by regulatory agencies, as calculated elsewhere [27]. On the other hand, the versatility of polyhistidine tails as tags in recombinant protein production and engineering [60] and their widespread use in affinity protein purification [61], useable at large scale [62], pose the bases for the simple development of a plethora of antigenic proteins formulated as secretory granules. Therefore, the results obtained here fully support the

concept of a platform for the fabrication of self-contained antigen-based depots intended for vaccination purposes and translatable to the industrial sector. In summary, synthetic secretory amyloids, inspired by the natural secretion granules, have potential in vaccinology by activating both the antigen-specific and the innate arms of the immune system, while providing a sustained source of the forming antigen through the progressive *in vivo* disintegration of a fully biocompatible material.

4. Conclusion

The subcutaneous administration of artificial secretory granules, fabricated with the SARS-CoV-2 RBD domain through a Zn-assisted protein cross-linking technology, attenuated hamster weight loss upon viral challenge and accelerated viral clearance, even in absence of adjuvant. Such unusual formulation, which mimics the endocrine-like slow protein release observed in the human hormonal system, appears to act through both antigen-dependent and antigen-independent routes, being the last one probably linked to the specific amyloidal architecture adopted by the secretory granules. These findings represent the first evaluation of an antigen-based secretory granule formulation in a real vaccination scenario against an infectious virus, and they open a door to explore a new category of functional amyloidal materials with combined secretory and immunomodulating properties.

CRediT authorship contribution statement

Eloi Parladé: Investigation. **Ferran Tarrés-Freixas:** Investigation. **Marianna T.P. Favaro:** Investigation. **Jara Lascorz:** Investigation. **Merce Márquez-Matínez:** Investigation. **Rosa Mendoza:** Investigation. **José Luís Corchero:** Investigation. **Guillermo Cantero:** Investigation. **Núria Roca:** Investigation. **Mónica Pérez:** Investigation. **Neus Ferrer-Miralles:** Investigation. **Esther Vazquez:** Investigation. **Joaquim Segalés:** Conceptualization, Investigation. **Júlia Vergara-Alert:** Conceptualization, Investigation. **Antonio Villaverde:** Writing – original draft, Conceptualization.

Declaration of competing interest

The authors declare the following financial interests/personal relationships which may be considered as potential competing interests: Esther Vázquez and Antonio Villaverde (and other inventors) have applied for a patent covering the immunogenic potential of artificial secretory granules.

Acknowledgements

The project was mainly funded by AGAUR (grant number 2020PANDE00003) and CIBER-Consorcio Centro de Investigación Biomédica en Red- (grant number CB06/01/0014), through the Instituto de Salud Carlos III, Ministerio de Ciencia e Innovación, within the intramural project NANOSARS (to E.P.). We also gratefully acknowledge the support from AEI for the development of multimeric recombinant drugs (grant numbers PID2019-105416RB-I00/AEI/10.13039/501100011033 and PDC2022-133858-I00 to E.V., PID2019-107298RB-C22/AEI/10.13039/501100011033 to N.F.-M., PID2020-116174RB-I00 to A.V. and PID2022-1368450 OB-10/AEI/10.13039/501100011033 to A.V. and E.V.). Our team also received support from AGAUR for our activities in drug design (grant number 2021SGR00092 to A.V.). Protein production was partially performed by the ICTS "NANBIOSIS", more specifically by the Protein Production Platform of CIBER in Bioengineering, Biomaterials & Nanomedicine (CIBER-BBN)/IBB, at the UAB (http://www.nanbiosis.es/portfolio/u1-protein-production-platform-ppp). IRTA is supported by CERCA Programme/Generalitat de Catalunya. The authors also acknowledge the invaluable assistance of the animal caretakers at the BSL3 facility at IRTA.

Data availability

Data will be made available on request.

References

[1] R. Vaishya, V. Khurana, S. Patel, A.K. Mitra, Long-term delivery of protein therapeutics, Expet Opin. Drug Deliv. 12 (2015), https://doi.org/10.1517/17425247.2015.961420, 415-40.
[2] P. Mandhar, G. Joshi, Development of sustained release drug delivery system: a review, asian pacific, J. Health Sci. 2 (2015) 179–185, https://doi.org/10.21276/apjhs.2015.2.1.31.
[3] P. Prajapat, D. Agrawal, G. Bhaduka, A brief overview of sustained released drug delivery system, Journal of Applied Pharmaceutical Research 10 (2022) 05–11, https://doi.org/10.18231/j.joapr.2022.10.3.5.11.
[4] S. Diksha, D. Dhruv, D.N. Prasad, H. Mansi, Sustained release drug delivery system with the role of natural polymers: a review, J. Drug Deliv. Therapeut. 9 (2019), 913-2, https://jddtonline.info/index.php/jddt/article/view/2859.
[5] F. Rizzo, N.S. Kehr, Recent advances in injectable hydrogels for controlled and local drug delivery, Adv. Healthcare Mater. 10 (2021) 2001341, https://doi.org/10.1002/adhm.202001341.
[6] P. Gupta, K. Vermani, S. Garg, Hydrogels: from controlled release to pH-responsive drug delivery, Drug Discov. Today 7 (2002), https://doi.org/10.1016/S1359-6446(02)02255-9, 569-79.
[7] K.E. Uhrich, S.M. Cannizzaro, R.S. Langer, K.M. Shakesheff, Polymeric systems for controlled drug release, Chem. Rev. 99 (1999) 3181–3198, https://doi.org/10.1021/cr940351u.
[8] J. Shen, J. Wolfram, M. Ferrari, H. Shen, Taking the vehicle out of drug delivery, Mater. Today 20 (2017) 95–97, https://doi.org/10.1016/j.mattod.2017.01.013.
[9] S.A. Levkovich, E. Gazit, D. Laor Bar-Yosef, Two decades of studying functional amyloids in microorganisms, Trends Microbiol. 29 (2021) 251–265, https://doi.org/10.1016/j.tim.2020.09.005.
[10] A. De Marco, N. Ferrer-Miralles, E. Garcia-Fruitós, A. Mitraki, S. Peternel, U. Rinas, M.A. Trujillo-Roldán, N.A. Valdez-Cruz, E. Vázquez, A. Villaverde, Bacterial inclusion bodies are industrially exploitable amyloids, FEMS Microbiol. Rev. 43 (2019) 53–72, https://doi.org/10.1093/femsre/fuy038.
[11] A.V. Sergeeva, A.P. Galkin, Functional amyloids of eukaryotes: criteria, classification, and biological significance, Curr. Genet. 66 (2020) 849–866, https://doi.org/10.1007/s00294-020-01079-7.
[12] R.S. Jacob, S. Das, S. Ghosh, A. Anoop, N.N. Jha, T. Khan, P. Singru, A. Kumar, S. K. Maji, Amyloid formation of growth hormone in presence of zinc: relevance to its storage in secretory granules, Sci. Rep. 6 (2016) 1–18, https://doi.org/10.1038/srep23370.
[13] L. Khemtemourian, F. Antoniciello, B.R. Sahoo, M. Decossas, S. Lecomte, A. Ramamoorthy, Investigation of the effects of two major secretory granules components, insulin and zinc, on human-IAPP amyloid aggregation and membrane damage, Chem. Phys. Lipids 237 (2021) 105083, https://doi.org/10.1016/j.chemphyslip.2021.105083.
[14] L.C.S. Erthal, A.F. Marques, F.C.L. Almeida, G.L.M. Melo, C.M. Carvalho, L. C. Palmieri, K.M.S. Cabral, G.N. Fontes, L.M.T.R. Lima, Regulation of the assembly and amyloid aggregation of murine amylin by zinc, Biophys. Chem. 218 (2016) 58–70, https://doi.org/10.1016/j.bpc.2016.09.008.
[15] G. Cereghetti, S. Saad, R. Dechant, M. Peter, Reversible, functional amyloids: towards an understanding of their regulation in yeast and humans, Cell Cycle 17 (2018) 1545–1558, https://doi.org/10.1080/15384101.2018.1480220.
[16] A. Anoop, S. Ranganathan, B. Das Dhaked, N.N. Jha, S. Pratihar, S. Ghosh, S. Sahay, S. Kumar, S. Das, M. Kombrabail, K. Agarwal, R.S. Jacob, P. Singru, P. Bhaumik, R. Padinhateeri, A. Kumar, S.K. Maji, Elucidating the role of disulfide bond on amyloid formation and fibril reversibility of somatostatin-14: relevance to its storage and secretion, J. Biol. Chem. 289 (2014), https://doi.org/10.1074/jbc.M114.548354, 16884-903.
[17] S.K. Maji, M.H. Perrin, M.R. Sawaya, S. Jessberger, K. Vadodaria, R.A. Rissman, P. S. Singru, K.P.R. Nilsson, R. Simon, D. Schubert, D. Eisenberg, J. Rivier, P. Sawchenko, W. Vale, R. Riek, Functional amyloids as natural storage of peptide hormones in pituitary secretory granules, Science 325 (2009) 328–332, https://doi.org/10.1126/SCIENCE.1173155/SUPPL_FILE/MAJI.SOM.PDF, 1979.
[18] W.C. Hymer, W.J. Kraemer, Resistance exercise stress: theoretical mechanisms for growth hormone processing and release from the anterior pituitary somatotroph, Eur. J. Appl. Physiol. 123 (2023) 1867–1878, https://doi.org/10.1007/s00421-023-05263-8.
[19] J.M. Sánchez, H. López-Laguna, P. Álamo, N. Serna, A. Sánchez-Chardi, V. Nolan, O. Cano-Garrido, I. Casanova, U. Unzueta, E. Vazquez, R. Mangues, A. Villaverde, Artificial inclusion bodies for clinical development, Adv. Sci. 7 (2020), 1902420, doi:10.1002/advs.201902420.
[20] J.M. Sánchez, H. López-Laguna, E. Parladé, A. Di Somma, A.L. Livieri, P. Álamo, R. Mangues, U. Unzueta, A. Villaverde, E. Vázquez, Structural stabilization of clinically oriented oligomeric proteins during their transit through synthetic secretory amyloids, Adv. Sci. (2024) e2309427, https://doi.org/10.1002/advs.202309427.
[21] P.S. Dannies, Prolactin and growth hormone aggregates in secretory granules: the need to understand the structure of the aggregate, Endocr. Rev. 33 (2012) 254–270, https://doi.org/10.1210/er.2011-1002.
[22] M. Tp Favaro, H. López-Laguna, E. Voltà-Durán, L. Alba-Castellon, J.M. Sánchez, I. Casanova, U. Unzueta, R. Mangues, A. Villaverde, E. Vázquez, Lyophilization of

biomimetic amyloids preserves their regulatable, endocrine-like functions for nanoparticle release, Appl. Mater. Today 39 (2024) 102348, https://doi.org/10.1016/j.apmt.2024.102348.
[23] M.V. Céspedes, O. Cano-Garrido, P. Álamo, R. Sala, A. Gallardo, N. Serna, A. Falgàs, E. Voltà-Durán, I. Casanova, A. Sánchez-Chardi, H. López-Laguna, L. Sánchez-García, J.M. Sánchez, U. Unzueta, E. Vázquez, R. Mangues, A. Villaverde, Engineering secretory amyloids for remote and highly selective destruction of metastatic foci, Adv. Mater. 32 (2020), 1907348, doi:10.1002/adma.201907348.
[24] T.Y. Chen, W.J. Cheng, J.C. Horng, H.Y. Hsu, Artificial peptide-controlled protein release of Zn2+-triggered, self-assembled histidine-tagged protein microparticle, Colloids Surf. B Biointerfaces 187 (2020), 110644, doi:10.1016/j.colsurfb.2019.110644.
[25] P. Álamo, E. Parladé, H. López-Laguna, E. Voltà-Durán, U. Unzueta, E. Vazquez, R. Mangues, A. Villaverde, Ion-dependent slow protein release from in vivo disintegrating micro-granules 28 (2021), https://doi.org/10.1080/10717544.2021.1998249, 2383-239.
[26] H. López-Laguna, E. Parladé, P. Álamo, J.M. Sánchez, E. Voltà-Durán, N. Serna, L. Sánchez-García, O. Cano-Garrido, A. Sánchez-Chardi, A. Villaverde, R. Mangues, U. Unzueta, E. Vázquez, H, In Vitro Fabrication of Microscale Secretory Granules, Adv. Funct. Mater. 2021, doi:10.1002/adfm.202100914.
[27] H. López-Laguna, J. Sánchez, U. Unzueta, R. Mangues, E. Vázquez, A. Villaverde, Divalent cations: a molecular glue for protein materials, Trends Biochem. Sci. 45 (2020), https://doi.org/10.1016/j.tibs.2020.08.003.
[28] H. López-Laguna, U. Unzueta, O. Conchillo-Solé, A. Sánchez-Chardi, M. Pesarrodona, O. Cano-Garrido, E. Voltà, L. Sánchez-García, N. Serna, P. Saccardo, R. Mangues, A. Villaverde, E. Vázquez, Assembly of histidine-rich protein materials controlled through divalent cations, Acta Biomater 83 (2019) 257–264, https://doi.org/10.1016/j.actbio.2018.10.030.
[29] H. López-Laguna, J.M. Sánchez, J.V. Carratalá, M. Rojas-Peña, L. Sánchez-García, E. Parladé, A. Sánchez-Chardi, E. Voltà-Durán, N. Serna, O. Cano-Garrido, S. Flores, N. Ferrer-Miralles, V. Nolan, A. de Marco, N. Roher, U. Unzueta, E. Vazquez, A. Villaverde, Biofabrication of functional protein nanoparticles through simple His-tag engineering, ACS Sustain. Chem. Eng. 9 (2021) 12341–12354, https://doi.org/10.1021/acssuschemeng.1c04256.
[30] N. Serna, A. Falgàs, A. García-León, U. Unzueta, Y. Núñez, A. Sánchez-Chardi, C. Martínez-Torró, R. Mangues, E. Vazquez, I. Casanova, A. Villaverde, Time-prolonged release of tumor-targeted protein–MMAE nanoconjugates from implantable hybrid materials, Pharmaceutics 14 (2022) 192, https://doi.org/10.3390/pharmaceutics14010192.
[31] N. Serna, O. Cano-Garrido, J.M. Sánchez, A. Sánchez-Chardi, L. Sánchez-García, H. López-Laguna, E. Fernández, E. Vázquez, A. Villaverde, Release of functional fibroblast growth factor-2 from artificial inclusion bodies, J. Control. Rel. 327 (2020), https://doi.org/10.1016/j.jconrel.2020.08.007. https://doi.org/10.1016/j.jconrel.2020.08.007.
[32] H. López-Laguna, P.M. Tsimbouri, V. Jayawarna, I. Rigou, N. Serna, E. Voltà-Durán, U. Unzueta, M. Salmeron-Sanchez, E. Vázquez, M.J. Dalby, A. Villaverde, Hybrid micro-/nanoprotein platform provides endocrine-like and extracellular matrix-like cell delivery of growth factors, ACS Appl. Mater. Interfaces (2024) 32930–32944, https://doi.org/10.1021/acsami.4c01210.
[33] N. Serna, H. López-Laguna, P. Aceituno, M. Rojas-Peña, E. Parladé, E. Voltà-Durán, C. Martínez-Torró, J.M. Sánchez, A. Di Somma, J.V. Carratalá, A.L. Livieri, N. Ferrer-Miralles, E. Vázquez, U. Unzueta, N. Roher, A. Villaverde, Efficient delivery of antimicrobial peptides in an innovative, slow-release pharmacological formulation, Pharmaceutics 15 (2023) 2632, https://doi.org/10.3390/pharmaceutics15112632.
[34] P. Álamo, E. Parladé, M.T.P. Favaro, A. Gallardo, R. Mendoza, L.C.S. Ferreira, N. Roher, R. Mangues, A. Villaverde, E. Vázquez, Probing the biosafety of implantable artificial secretory granules for the sustained release of bioactive proteins, ACS Appl. Mater. Interfaces 15 (2023) 39167–39175, https://doi.org/10.1021/acsami.3c08643.
[35] M.T.P. Favaro, P. Alamo, N. Roher, M. Chillon, J. Lascorz, M. Márquez, J. L. Corchero, R. Mendoza, C. Martínez-Torró, N. Ferrer-Miralles, L.C.S. Ferreira, R. Mangues, E. Vázquez, E. Parladé, A. Villaverde, Zinc-assisted microscale granules made of the SARS-CoV-2 spike protein trigger neutralizing, antivirus antibody responses, ACS Mater. Lett. (2024) 954–962, https://doi.org/10.1021/acsmaterialslett.3c01643.
[36] L. Bosch-Camós, C. Martínez-Torró, H. López-Laguna, J. Lascorz, J. Argilaguet, A. Villaverde, F. Rodríguez, E. Vázquez, Nanoparticle-based secretory granules induce a specific and long-lasting immune response through prolonged antigen release, Nanomaterials 14 (2024) 435, https://doi.org/10.3390/nano14050435.
[37] I. Quast, D. Tarlinton, Time is of the essence for vaccine success, Nat. Immunol. 23 (2022) 1517–1519, https://doi.org/10.1038/s41590-022-01347-3.
[38] M.J. Hogan, N. Pardi, mRNA vaccines in the COVID-19 pandemic and beyond, Annu. Rev. Med. 73 (2022) 17–39, https://doi.org/10.1146/annurev-med-042420-112725.
[39] J. Han, J. Yin, X. Wu, D. Wang, C. Li, Environment and COVID-19 incidence: a critical review, J. Environ. Sci. 124 (2023) 933–951, https://doi.org/10.1016/j.jes.2022.02.016.
[40] Y. Hu, J. Sun, Z. Dai, H. Deng, X. Li, Q. Huang, Y. Wu, L. Sun, Y. Xu, Prevalence and severity of corona virus disease 2019 (COVID-19): a systematic review and meta-analysis, J. Clin. Virol. 127 (2020) 104371, https://doi.org/10.1016/j.jcv.2020.104371.
[41] P.V. Markov, M. Ghafari, M. Beer, K. Lythgoe, P. Simmonds, N.I. Stilianakis, A. Katzourakis, The evolution of SARS-CoV-2, Nat. Rev. Microbiol. 21 (2023) 361–379, https://doi.org/10.1038/s41579-023-00878-2.
[42] J.L. Corchero, M.T.P. Favaro, M. Márquez-Martínez, J. Lascorz, C. Martínez-Torró, J.M. Sánchez, H. López-Laguna, L.C. de Souza Ferreira, E. Vázquez, N. Ferrer-Miralles, A. Villaverde, E. Parladé, Recombinant proteins for assembling as nano- and micro-scale materials for drug delivery: a host comparative overview, Pharmaceutics 15 (2023) 1197, https://doi.org/10.3390/pharmaceutics15041197.
[43] C. Lei, J. Yang, J. Hu, X. Sun, On the calculation of TCID50 for quantitation of virus infectivity, Virol. Sin. 36 (2021) 141–144, https://doi.org/10.1007/s12250-020-00230-5.
[44] M. Brustolin, J. Rodon, M.L. Rodríguez de la Concepción, C. Ávila-Nieto, G. Cantero, M. Pérez, N. Te, M. Noguera-Julián, V. Guallar, A. Valencia, N. Roca, N. Izquierdo-Useros, J. Blanco, B. Clotet, A. Bensaid, J. Carrillo, J. Vergara-Alert, J. Segalés, Protection against reinfection with D614- or G614-SARS-CoV-2 isolates in golden Syrian hamster, Emerg. Microb. Infect. 10 (2021) 797–809, https://doi.org/10.1080/22221751.2021.1913974.
[45] E. Vidal, C. López-Figueroa, J. Rodon, M. Pérez, M. Brustolin, G. Cantero, V. Guallar, N. Izquierdo-Useros, J. Carrillo, J. Blanco, B. Clotet, J. Vergara-Alert, J. Segalés, Chronological brain lesions after SARS-CoV-2 infection in hACE2-transgenic mice, Vet. Pathol. 59 (2022) 613–626, https://doi.org/10.1177/03009858211066841.
[46] J. Abramson, J. Adler, J. Dunger, R. Evans, T. Green, A. Pritzel, O. Ronneberger, L. Willmore, A.J. Ballard, J. Bambrick, S.W. Bodenstein, D.A. Evans, C.-C. Hung, M. O'Neill, D. Reiman, K. Tunyasuvunakool, Z. Wu, A. Žemgulytė, E. Arvaniti, C. Beattie, O. Bertolli, A. Bridgland, A. Cherepanov, M. Congreve, A.I. Cowen-Rivers, A. Cowie, M. Figurnov, F.B. Fuchs, H. Gladman, R. Jain, Y.A. Khan, C.M. R. Low, K. Perlin, A. Potapenko, P. Savy, S. Singh, A. Stecula, A. Thillaisundaram, C. Tong, S. Yakneen, E.D. Zhong, M. Zielinski, A. Žídek, V. Bapst, P. Kohli, M. Jaderberg, D. Hassabis, J.M. Jumper, Accurate structure prediction of biomolecular interactions with AlphaFold 3, Nature (2024) 493–500, https://doi.org/10.1038/s41586-024-07487-w.
[47] Y. Ni, A. Alu, H. Lei, Y. Wang, M. Wu, X. Wei, Immunological perspectives on the pathogenesis, diagnosis, prevention and treatment of COVID-19, Molecular Biomedicine 2 (2021) 1–26, https://doi.org/10.1186/S43556-020-00015-Y, 2021 2:1.
[48] H. Aghamirza Moghim Aliabadi, R. Eivazzadeh-Keihan, A. Beig Parikhani, S. Fattahi Mehraban, A. Maleki, S. Fereshteh, M. Bazaz, A. Zolriasatein, B. Bozorgnia, S. Rahmati, F. Saberi, Z. Yousefi Najafabadi, S. Damough, S. Mohseni, H. Salehzadeh, V. Khakyzadeh, H. Madanchi, G.A. Kardar, P. Zarrintaj, M.R. Saeb, M. Mozafari, COVID-19: a systematic review and update on prevention, diagnosis, and treatment, MedComm (Beijing) 3 (2022) e115, https://doi.org/10.1002/MCO2.115.
[49] S.Y. Jung, K.W. Kang, E.Y. Lee, D.W. Seo, H.L. Kim, H. Kim, T.W. Kwon, H.L. Park, H. Kim, S.M. Lee, J.H. Nam, Heterologous prime–boost vaccination with adenoviral vector and protein nanoparticles induces both Th1 and Th2 responses against Middle East respiratory syndrome coronavirus, Vaccine 36 (2018) 3468–3476, https://doi.org/10.1016/J.VACCINE.2018.04.082.
[50] M. Ferranna, Causes and costs of global COVID-19 vaccine inequity, Semin. Immunopathol. 45 (2024) 469–480, https://doi.org/10.1007/S00281-023-00998-0/FIGURES/4.
[51] I. Wahl, H. Wardemann, Sterilizing immunity: understanding COVID-19, Immunity 55 (2022) 2231–2235, https://doi.org/10.1016/j.immuni.2022.10.017.
[52] A.S. Rosenberg, Effects of protein aggregates: an Immunologic perspective, AAPS J 8 (2006) E501–7, https://doi.org/10.1208/aapsj080359.
[53] N.B. Pham, W.S. Meng, Protein aggregation and immunogenicity of biotherapeutics, Int. J. Pharm. 585 (2020), 119523, doi:10.1016/j.ijpharm.2020.119523.
[54] K.D. Ratanji, J.P. Derrick, R.J. Dearman, I. Kimber, Immunogenicity of therapeutic proteins: influence of aggregation, J. Immunot. 11 (2014) 99–109, https://doi.org/10.3109/1547691X.2013.821564.
[55] E.M. Moussa, J.P. Panchal, B.S. Moorthy, J.S. Blum, M.K. Joubert, L.O. Narhi, E. M. Topp, Immunogenicity of therapeutic protein aggregates, J Pharm Sci 105 (2016) 417–430, https://doi.org/10.1016/j.xphs.2015.11.002.
[56] A.C.V.S.C. de Araujo, F. Mambelli, R.O. Sanches, F.V. Marinho, S.C. Oliveira, Current understanding of Bacillus calmette-guérin-mediated trained immunity and its perspectives for controlling intracellular infections, Pathogens 12 (2023) 1386, https://doi.org/10.3390/PATHOGENS12121386, 2023, Vol. 12, Page 1386.
[57] M.G. Netea, J. Domínguez-Andrés, L.B. Barreiro, T. Chavakis, M. Divangahi, E. Fuchs, L.A.B. Joosten, J.W.M. van der Meer, M.M. Mhlanga, W.J.M. Mulder, N. P. Riksen, A. Schlitzer, J.L. Schultze, C. Stabell Benn, J.C. Sun, R.J. Xavier, E. Latz, Defining trained immunity and its role in health and disease, Nat. Rev. Immunol. 20 (2020) 375–388, https://doi.org/10.1038/s41577-020-0285-6, 2020 20:6.
[58] J.M. Sanchez, H. López-Laguna, N. Serna, U. Unzueta, P.D. Clop, A. Villaverde, E. Vazquez, Engineering the performance of artificial inclusion bodies built of catalytic β-galactosidase, ACS Sustain. Chem. Eng. 9 (2021) 2552–2558, https://doi.org/10.1021/acssuschemeng.0c08345.
[59] E. Parladé, J.M. Sánchez, H. López-Laguna, U. Unzueta, A. Villaverde, E. Vázquez, Protein features instruct the secretion dynamics from metal-supported synthetic amyloids, Int. J. Biol. Macromol. 250 (2023) 126164, https://doi.org/10.1016/J.IJBIOMAC.2023.126164.
[60] H. López-Laguna, E. Voltà-Durán, E. Parladé, A. Villaverde, E. Vázquez, U. Unzueta, Insights on the emerging biotechnology of histidine-rich peptides,

Biotechnol. Adv. 54 (2022) 107817, https://doi.org/10.1016/J.BIOTECHADV.2021.107817.

[61] A. Spriestersbach, J. Kubicek, F. Schäfer, H. Block, B. Maertens, Purification of his-tagged proteins, Methods Enzymol. 559 (2015) 1–15, https://doi.org/10.1016/BS.MIE.2014.11.003.

[62] V. Gaberc-Porekar, V. Menart, Potential for using histidine tags in purification of proteins at large scale, Chem. Eng. Technol. 28 (2005) 1306–1314, https://doi.org/10.1002/CEAT.200500167.